Few-cycle fiber pulse compression and evolution of negative resonant radiation

2014 New J. Phys. 16 063017

(http://iopscience.iop.org/1367-2630/16/6/063017)

New Journal of Physics
The open access journal at the forefront of physics
Deutsche Physikalische Gesellschaft DPG | IOP Institute of Physics

Few-cycle fiber pulse compression and evolution of negative resonant radiation

J McLenaghan and F König
School of Physics and Astronomy, SUPA, University of St. Andrews, North Haugh, St. Andrews, KY16 9SS, UK
E-mail: fewk@st-andrews.ac.uk

Received 20 December 2013, revised 17 March 2014
Accepted for publication 16 April 2014
Published 10 June 2014
New Journal of Physics **16** (2014) 063017
doi:10.1088/1367-2630/16/6/063017

Abstract
We present experimental observations of the spectral expansion of fs-pulses compressing in optical fibers. Using the input pulse frequency chirp we are able to scan through the pulse compression spectra and observe in detail the emergence of negative-frequency resonant radiation (NRR), a recently discovered pulse instability coupling to negative frequencies. We observe how the compressing pulse is exciting NRR as long as it overlaps spectrally with the resonant frequency. Furthermore, we observe that optimal pulse compression can be achieved at an optimal input chirp and for an optimal fiber length. Our measurements are supported by simulations of the compressing pulse propagation. The results are important for Kerr-effect pulse compressors, to generate novel light sources, as well as for the observation of quantum vacuum radiation.

Keywords: resonant radiation, pulse compression, few-cycle pulses, analog horizon, negative frequency

1. Introduction

Negative resonant radiation (NRR) is a recently discovered dispersive wave generation process in nonlinear optical media [1]. It tranfers energy from a soliton to a dispersive wave under a phase matched process that couples positive soliton frequencies to negative frequencies [2]. It is a negative-frequency extension to the well known resonant radiation (RR), that couples positive

frequencies only [3, 4] and is an important part of supercontinuum generation [5–8]. RR is also important in various possible applications including photobiology [11], astrocomb generation [10], and the production of squeezed states [11].

NRR is particularly interesting as it demonstrates the necessity to include negative frequencies into the description of a field in nonlinear optics. Whilst negative frequencies are present in all electromagnetic fields they are typically ignored as they contain the same information as their corresponding positive frequencies. This can be seen by expressing a field A by Fourier transform,

$$A\left(z,\, t\right) = \frac{1}{2\pi}\int_{-\infty}^{\infty}\widetilde{A}\left(z,\, \omega\right)\exp\left(-\mathrm{i}\omega t\right)\mathrm{d}\omega. \tag{1}$$

Here $\widetilde{A}\left(z,\, \omega\right)$ has been integrated over both positive and negative frequencies. For a real field $\widetilde{A}\left(z,\, -\omega\right) = \widetilde{A}^{*}\left(z,\, \omega\right)$, i.e. the negative frequency part is determined by the positive frequency part. However, the interaction of postive and negative frequency components of a field can lead to qualitatively new phenomena such as NRR.

The mixing of positive and negative frequencies is a familiar concept in quantum field theory [12]. For example, it is behind the generation of Hawking radiation [13, 14]. Laboratory analogues of Hawking radiation [15] have been of great interest in recent decades and several different implementations have been suggested to study the effect using e.g. water waves [16], BECs [17], optical materials [18, 19], or superconducting circuits [20]. Interestingly, one analogue system also uses solitons in fibers. In this system the analogue Hawking effect is produced by scattering of the quantum vacuum at the optical event horizon [18]. NRR can also be described as the scattering of light at the horizon, however, here bright light from the pulse is scattered [21]. Although more light needs to be shed on the relation between these two effects, it is interesting to notice that they are occuring under similar experimental conditions: NRR is observed for extreme nonlinear pulse compression [2, 3] whilst the analogue Hawking radiation is expected to occur for extremely steep pulse fronts [18].

In order to measure how the NRR radiation is emerging from a compressing pulse, experimental control of the pulse compression is required. Various tools have been used to control pulse evolution and compression in a fiber including the tuning of the pulse wavelength, pulse length, pulse power, and changes in the fiber core size and in the fiber dispersion [22–25]. A variation of the pulse power effectively changes where in the fiber the pulse compresses, however, this method has a limited range determined by the onset of NRR and the maximum power available. In addition, the degree of spectral expansion and generation efficiency of the NRR are significantly affected in a nontrivial way. Having said that, the frequency chirp of the input pulse can lead to a delay of nonlinear pulse evolution. The dependence on chirp of various aspects of pulse evolution have been considered previously including the effect on supercontinuum generation [26–29] and spectral broadening [30, 31]. In the latter two papers the influence of chirp on spectral broadening was investigated numerically and experimentally for (50 fs) pulses. The results show an increased spectral broadening at the end of a (10 cm) piece of fiber when the input pulse chirp is positive and balanced by the total negative dispersion over the fiber length. This occurs because the input chirp must be compensated, delaying pulse compression. In this paper we present to the best of our knowledge the first detailed investigation of chirp looking beyond the idea of delayed pulse compression. We look at a regime of shorter pulses (<20 fs) and shorter fibers (<0.1 m) and find interesting effects

such as the increased degree of pulse compression for a small positive chirp compared to zero chirp. As in the papers mentioned above we see delayed pulse compression and use this as a convenient tool to observe the evolution of both the pulse and the NRR under near constant spectral expansion.

In this paper, firstly, we present simulations of the pulse evolution and compression. We investigate how the pulse chirp affects the pulse compression. Secondly, we present measurements of the pulse spectra and NRR spectra for variable pulse chirps. We give a detailed discussion of the observations and implications from our simulations. As a result, we observe that the pulse compression has a weak dependence on chirp, however, the chirp is able to delay or advance the pulse compression in the fiber in accordance with the expectation from dispersion cancellation. NRR is generated at the point in the fiber where the pulse starts to compress and generation ceases after compression is over and the pulse expands again. The amount of NRR detected at the end of the fiber is also affected by waveguide loss. Our observations are in qualitative agreement with the analytical description of NRR evolution in fibers [3, 2].

2. Resonant radiation

NRR and RR form as energy is transferred from a pulse, similar to a soliton, propagating in the anomalous dispersion region of an optical fiber to light in the normal dispersion region. Light propagation in the fiber is governed by the generalized nonlinear Schrödinger equation (GNLSE) [7]. Neglecting absorption and higher order terms, except dispersion, the propagation equation becomes

$$\frac{\partial A}{\partial Z} - \mathrm{i}D\left(\mathrm{i}\frac{\partial}{\partial T}\right)A = \mathrm{i}\gamma\left|A\right|^2 A, \tag{2}$$

where $A\left(Z, T\right)$ is the pulse envelope, γ is the nonlinear parameter of the fiber, and $F.T.\left[D\left(\mathrm{i}\frac{\partial}{\partial T}\right)\right] = \widetilde{D}\left(\omega\right) = \sum_{n\geqslant 2}\frac{\beta_n}{n!}\omega^n$ represents the second and higher order group velocity dispersion (GVD). $T = t - z/v_\mathrm{g}$ and $Z = z/v_\mathrm{g}$ are time and space coordinates in a reference frame moving with the group velocity v_g of the pulse.

An important parameter characterizing soliton amplitudes is the soliton order N, given by $N^2 = \gamma P_0 T_0^2/\left|\beta_2\right|$ where P_0 and T_0 are the soliton peak power and length, respectively. This parameter can also be used for soliton-like pulses in our experiments. For higher ($N > 1$) order solitons the instabilities caused by higher order effects lead to fission into N fundamental ($N = 1$) solitons [32, 33]. The higher order dispersion is perturbing each of the produced solitons, which consequently will radiate dispersive RR and NRR. The radiation generated at different times as the pulse propagates along the fiber interferes constructively if the following momentum conserving phase matching condition is satisfied [3, 34, 35],

$$\sum_{n\geqslant 2}\frac{\beta_n}{n!}\left(\omega - \omega_\mathrm{S}\right)^n = \frac{\left(2N-1\right)^2\gamma P_0}{2N^2}, \tag{3}$$

where ω and ω_S are the phase matched radiation (RR or NRR) and pulse frequencies, respectively. Note that the GNLSE, if used with complex fields of both positive and negative

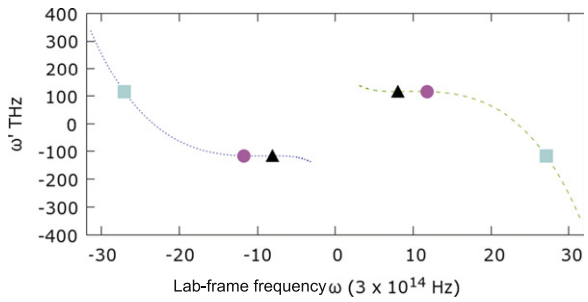

Figure 1. Co-moving frame dispersion relation for positive (- - - -) and negative (……) laboratory frequencies. The soliton (△), RR (○) and NRR (□) are indicated. Fiber NL-1.5-590, NKT Photonics.

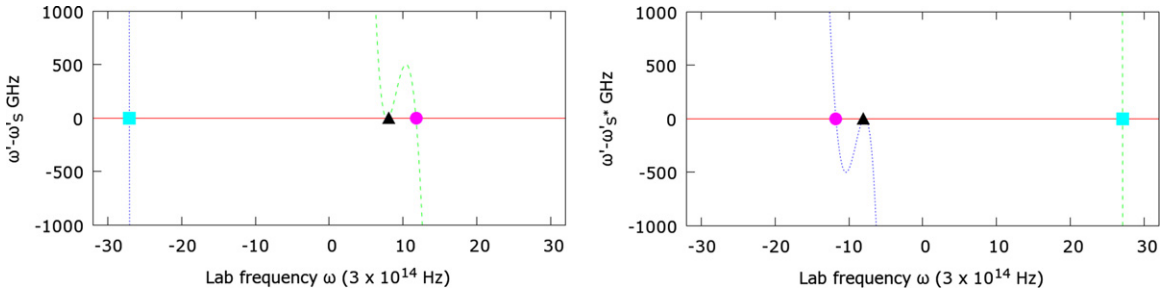

(a) Positive ω' (b) Negative ω'

Figure 2. Co-moving frame dispersion relation for positive (- - - -) and negative (……) laboratory frequencies as in figure 1. Zoomed view around (a) ω'_{S} and (b) $-\omega'_{\mathrm{S}}$. The soliton (△), RR (○) and NRR (□) are indicated.

frequency components, can be derived without the slowly varying envelope approximation, and the phase matching condition holds for both RR and NRR. Alternatively, the complex field can be constrained to positive frequencies only, which results in an envelope equation for the analytic signal, different from the GNLSE. In this case two phase matching conditions are found for RR and NRR, respectively [1]. In order to graphically find the phase matched frequencies we express (3) as a frequency conservation in the co-moving frame [1, 18]

$$\omega'_{\mathrm{S}} = \omega', \tag{4}$$

where ω' is the (Galilean) co-moving frame frequency of the pulse and NRR, respectively, given by $\omega' = \omega - v_{\mathrm{g}}\left(\beta\left(\omega\right) + \beta_{\mathrm{nl}}\right)$. β is related to the refractive index by $\beta = n\left(\omega\right)\omega/c$ and β_{nl} is the nonlinear contribution to the propagation constant due to the soliton pulse. Figure 1 shows the dispersion relation of our fiber in the co-moving frame ($\beta_{\mathrm{nl}} = 0$). Figure 2 (a) shows a closer view of the top part of the dispersion relation around the soliton pulse co-moving frame frequency ω'_{S}. Figure 2(b) shows the lower part of the dispersion relation plotted around $-\omega'_{\mathrm{S}}$. There are two branches to the relation seen in each of the three plots, one with positive and one with negative laboratory frequency. Marked with a symbol in figure 2(a) are the soliton, the RR wavelength, and a third solution, the NRR on the other branch. In figure 2(b) the complex

conjugate fields are displayed. This shows that the soliton can excite two other waves, each of which is a real-numbered field, one with a positive and one with a negative frequency.

3. Numerical simulations

In order to understand the pulse evolution, i.e. the pulse compression and spectral expansion, under the influence of pulse chirp we numerically simulated the pulse amplitude propagation using a split step Fourier simulation tool [37]. The tool simulates the pulse envelope propagation described by the GNLSE, but for positive frequencies only. Therefore, it will model the pulse propagation and RR generation, but will not produce NRR.

We used a 12 fs (FWHM) hyperbolic secant pulse centered at 800 nm wavelength with the amplitude of an $N = 2.25$ soliton similar to the experiment. The frequency chirp of the initial pulse was varied and the evolutions of the pulse spectrum and the peak power were recorded. Because we chose a highly nonlinear fiber, the pulse compresses over a few mm. Hence effects taking place over longer propagation distances such as stimulated Raman scattering are not considered in detail. We simulated the propagation of pulses through a fiber with the dispersion profile shown in figures 1 and 2.

Pulse compression in an optical fiber occurs due to the interplay between self-phase modulation (SPM) and GVD. SPM broadens the pulse spectrum and generates a positive chirp, i.e. long wavelengths lead and short wavelengths trail. Anomalous GVD slows the long wavelengths and speeds up short wavelengths, resulting in pulse compression (compression only occurs across the central region of the pulse where both the SPM and GVD induced chirps are approximately linear). Adding, via pulse dispersion, a frequency chirp to the input pulse has two key effects on the pulse compression. Firstly, the distance at which the pulse compresses to its shortest length is modified. If the initial chirp is positive, then the anomalous fiber GVD acts to reduce the chirp and increase the pulse peak power before the nonlinear dynamics fully compresses the pulse. Hence positive input chirp delays compression further along the fiber. Secondly, the amount by which the pulse compresses can be either enhanced or reduced.

We started our simulations to verify this qualitative behaviour. In figure 3 a series of spectral evolutions is displayed for different input chirps (in units of fs^2). For comparison, the fibers we use in experiments have dispersions between 20 $fs^2\ mm^{-1}$ and 40 $fs^2\ mm^{-1}$. If no chirp is applied, the initial pulse spectrum centered in the near infrared can be seen to expand over three octaves within the first 2 mm of propagation. The spectrum then contracts again at 2.5 mm as the pulse continues to propagate. This corresponds to the temporal evolution of the pulse given in figure 4. If a positive input chirp is applied, figure 3 shows that the distance at which the pulse compresses and the spectrum expands increases accordingly. In addition, the extent of spectral broadening reduces.

In the time domain, as shown in figure 4, the peak power first increases to a maximum at the maximal spectral expansion and then reduces again as the pulse broadens in time. The dependence of this maximum peak power on input chirp is displayed in figure 5 for a set of input pulse parameters. The solid line in each of the sub-figures representss a 12 fs, $N = 2.25$ input pulse. Clearly, the peak power increases with amplitude N and reduces with pulse duration. Also, the maximum peak power decreases eventually for large chirp for all amplitudes and pulse durations shown. For all traces in figure 5 there is a finite optimal input chirp that leads to maximum pulse compression. The enhancement seems to be best for the 12 fs pulse

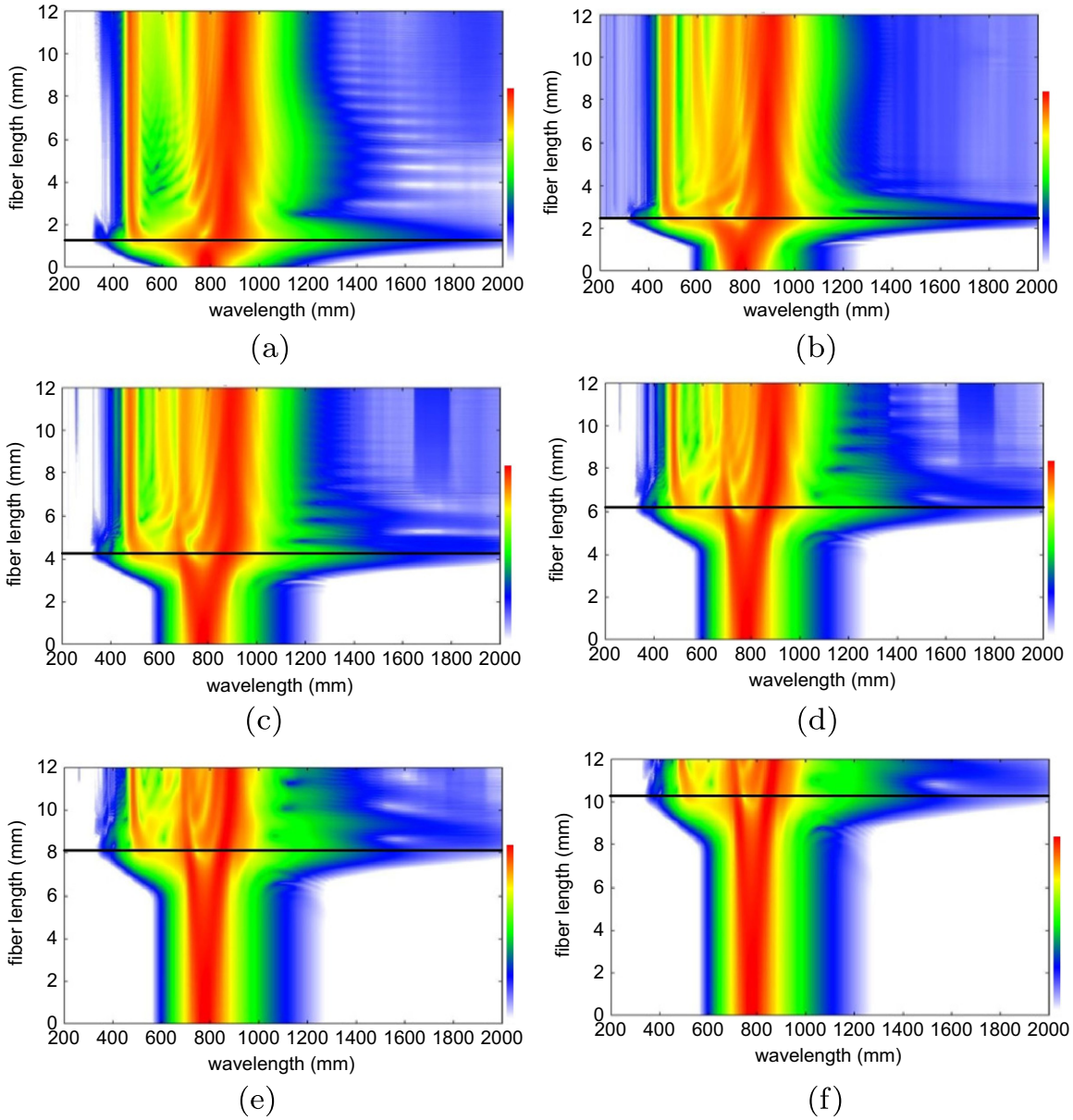

Figure 3. Pulse spectral evolution during propagation for different input pulse chirps ((a): 0 fs^2; (b): 100 fs^2; (c): 170 fs^2; (d): 240 fs^2; (e): 305 fs^2; (f): 375 fs^2). The color scale covers a dynamic range of 80 dB. The horizontal line indicates the maximum spectral broadening.

duration. Figure 6 shows how this nonzero chirp depends on pulse amplitude. For all amplitudes, there is a positive chirp leading to an improvement of the pulse compression, which is particularly pronounced for smaller pulse amplitudes. For the N = 2.25 pulse we also increased the pulse length and found the optimum chirp to slightly decrease from 80 fs^2 to a steady value of around 60 fs^2. The improvement in the maximum peak power rose to a maximum of 18% for a 50 fs pulse (results not shown). For our fiber a chirp of 375 fs^2 would change the distance of compression from close to zero to the end of our longest fibers of 14 mm

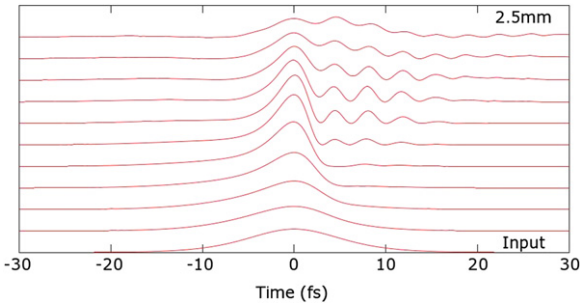

Figure 4. Evolution of the pulse temporal envelope as the pulse propagates from 0 mm to 2.5 mm along the fiber. The pulse has zero initial chirp.

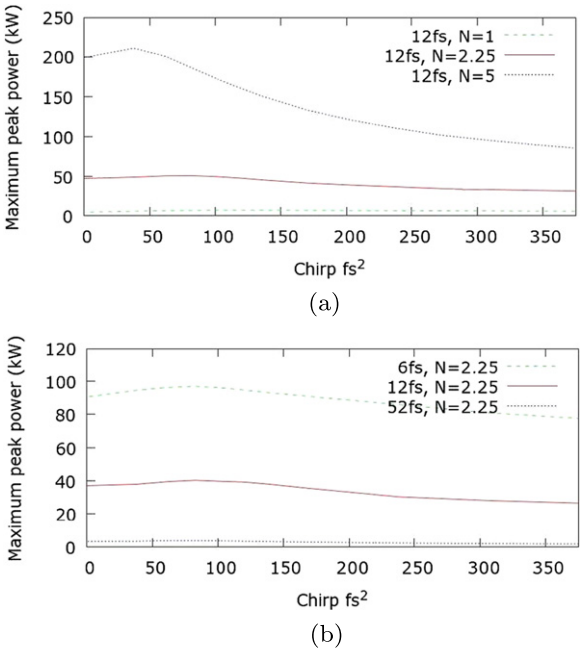

Figure 5. Maximum peak power during pulse compression as a function of input chirp. Results are for different input pulse soliton orders (a: $N = 5$ ⋯⋯; $N = 2.25$ ———; $N = 1$ ⋯⋯) and pulse lengths (b: 6 fs - - - -; 12 fs ———; 52 fs⋯⋯).

length. According to figure 5, over the same range the maximum peak power increases first by 9% and then falls to 36% below the unchirped compression. This means that as the compression is delayed along the fiber, there is only a small variation in compression efficiency. Effectively, the pulse compression can be observed in its different stages at the fiber end by small variations of the pulse chirp around an offset chirp compensating the fiber dispersion. If instead the pulse power was used to move the compression point from the start to the end of the fiber, then the variation in power required would be considerably larger for similar pulse parameters. For example, for an input chirp of 240 fs^2 and a 12 fs pulse, the input power would have to vary by a factor of 25.

In addition to investigating the effects of input chirp, pulse power, and pulse length on pulse compression, we turn on and off higher order effects such as self-steepening and the

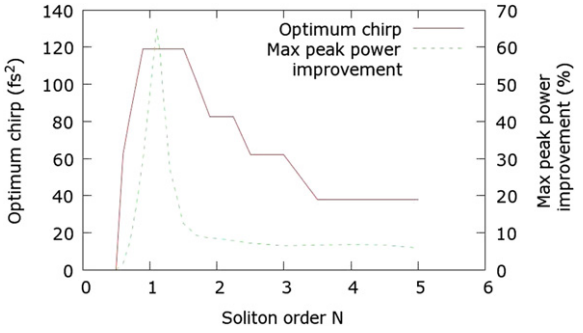

Figure 6. Optimum chirp for pulse compression as a function of soliton order N (———); maximum peak power enhancement using the optimum chirp compared to zero chirp (- - - -).

Raman effect. We find that the self-steepening has a negligible effect on the compression distance and slightly reduces both the spectral expansion and the maximum peak power. The Raman effect slightly increases the propagation distance before the compression point but has a negligible effect on the spectral expansion or the maximum peak power. Also, as explained above, no NRR production is observed due to the nature of our simulation tool.

Summarizing, the simulations show that, for a wide range of input pulse parameters, chirp can be used to move the pulse compression along the fiber. The accompanying changes in the degree of pulse compression must be taken into account but are small enough to allow for a qualitative investigation of the pulse and NRR evolution. The origin of these changes is not fully understood and is to be investigated elsewhere. Furthermore, a small positive input chirp leads to maximal pulse compression.

4. Experiment

We investigate two principal aspects of the pulse and NRR evolution. The first is the pulse spectral expansion. In order to excite the NRR in the UV (figure 2), the driving input pulse in the IR must broaden its spectrum extensively to reach the NRR wavelength. The spectral broadening is a transient effect during the pulse compression. Therefore, in order to measure the extent of the broadening into the UV we use the input chirp to move each stage of the pulse compression, respectively, to the fiber end. The second aspect is the evolution of the NRR itself, which is generated when the pulse compresses. By moving the compression point again we can change the distance propagated by the NRR between its first generation and the fiber end and observe its evolution. In addition we see how the variation in compression efficiency with chirp affects the generation of NRR.

Figure 7 shows the experimental setup. We use 800 nm pulses from a mode-locked Ti: Sapphire laser (FemtoSource Rainbow). A short pass filter at 695 nm cleans up the spectrum, resulting in a pulse length (FWHM) of 12 fs for the unchirped pulse and a bandwidth of over 200 nm. The pulses are coupled into a photonic crystal fiber (PCF) (NL-1.5-590, NKT Photonics) with a zero-dispersion wavelength at about 685 nm and a GVD of $-33\ \mathrm{ps}^2\ \mathrm{km}^{-1}$ at 800 nm. The fiber has a specified mode field diameter of 1.34 μm and a nonlinear coefficient of $136\ \left(\mathrm{W\ km}\right)^{-1}$ at 780 nm. The laser output is linearly polarized and all PCFs are rotated so as to

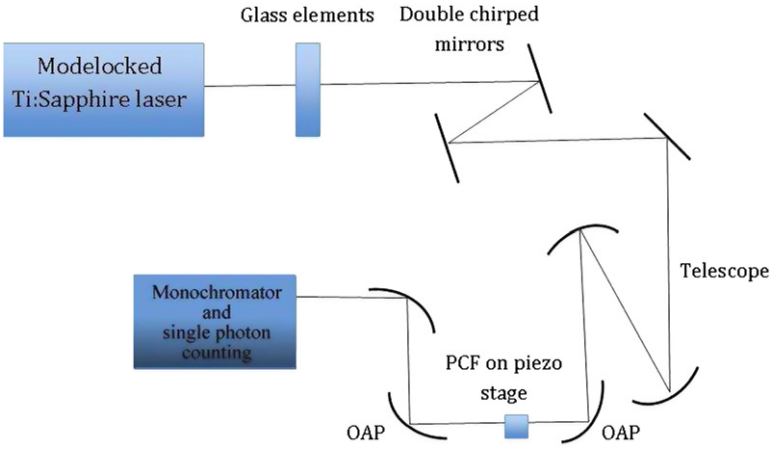

Figure 7. Experimental setup: BK7 glass plates and wedges were used to control the input pulse chirp.

excite only one polarization axis. The laser wavelength is situated in the anomalous dispersion region of the PCF, which allows for the formation of solitons. A dispersion optimized coupling into the PCF is achieved using of off-axis parabolic mirrors. UV spectra are recorded using a monochromator with a photomultiplier tube. Dispersion is managed up to second order by glass elements in the beam and a pair of doubly chirped mirrors (DCMs).

The dispersive pulse chirp C leads to an increase in the pulse length and a variation in the instantaneous frequency across the pulse. It is quantified by $C = \sum_i \beta_{2i} z_i + \mathrm{GDD}_{\mathrm{DCM}}$, where β_{2i} and z_i are the GVD and beam path distances for each dispersive optical element before the fiber, and $\mathrm{GDD}_{\mathrm{DCM}}$ is the negative group delay dispersion (GDD) introduced by the DCMs.

We use different section lengths of PCF from 1 mm to 14 mm. For the 1 mm and 2 mm lengths the laser power prior to coupling into the PCF is 100 mW, and for the other lengths it is 80 mW. The coupling efficiency into the PCF is around 25%, varying between fiber samples. This results in a soliton order of approximately $N = 2.25$.

5. Spectral expansion

The contour plots in figure 8 show the UV spectra as a function of the input chirp for four fiber lengths. For each length of fiber there is a particular input chirp (indicated by a black line) for which the spectrum becomes maximally broad. For longer fibers this broadening is observed for higher input chirps. It is a transient effect that disappears at other chirps, demonstrating the transient spectral expansion as the pulse compresses. Interestingly this shows that the pulse broadens its spectrum from the IR to the UV by self-compression. Table 1 compares input pulse chirps that lead to observable pulse compression at the fiber end, based on different mechanisms. 'Linear' indicates the chirp that would compensate the linear dispersion of the full length of the fiber. In order to facilitate comparison with experimental results the errors indicate a range of values for slightly longer or shorter fibers, reflecting the experimental uncertainty in the fiber length. The principal nonlinear effect in fibers is SPM, which broadens the spectrum, leading to a faster compression in anomalous dispersion. Thus our numerical simulations of the nonlinear behaviour result in larger input chirps for compression at the fiber end. As previously

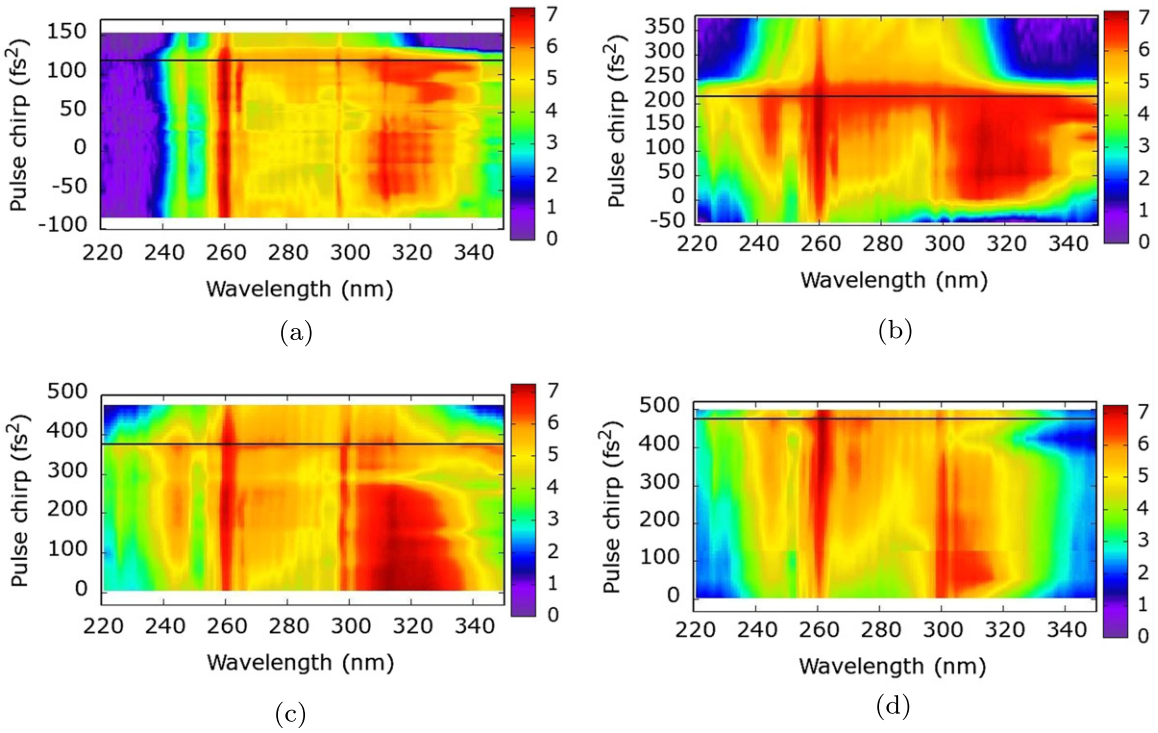

Figure 8. Contour plots of spectra as the input pulse chirp is varied, for different fiber lengths (a): 2 mm; (b): 6 mm; (c): 10 mm; (d): 14 mm. The horizontal line indicates the largest spectral broadening due to pulse compression. The color scale covers 70 dB.

Table 1. Comparison of input pulse chirps leading to pulse compression at the end of the fiber as deduced from: linear optics chirp compensation $L\beta_2$; numerically simulated pulse compression; observed UV spectral broadening; observed generation of NRR.

PCF length (mm)	Linear (fs^2)	Full simulation (fs^2)	UV expt. (figure 8) (fs^2)	NRR expt. (figure 9) (fs^2)
2	54 ± 13	96 ± 22	117	90
6	161 ± 13	234 ± 30	214	154
10	269 ± 13	376 ± 44	374	374
14	377 ± 13	518 ± 58	474	474

mentioned the simulations were run using different input powers. Increasing the power enhances the effect of SPM and results in an even larger input chirp for compression at the fiber end. The error values for the simulation results in table 1 indicate how the chirp value varies for a small range of input pulse powers. This allows comparison between simulation and experiment by taking into account the uncertainty in the exact experimental coupling efficiency into each piece of fiber. Next, we compare this chirp to the one used to observe the broadband expansion into the UV. Simulation and experimental results agree well within the errors.

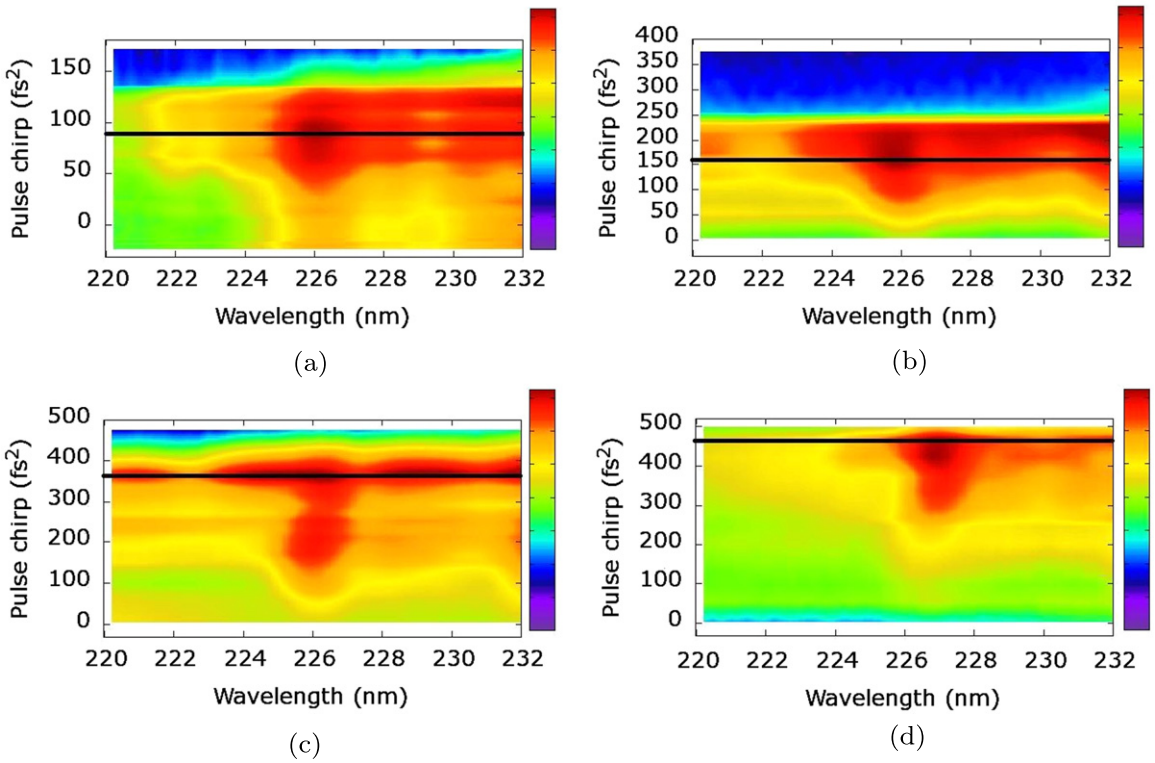

Figure 9. Contour plots showing the NRR as the input chirp is varied; the peak at approximately 226 nm is the NRR. Logarithmic scale, peak counts as indicated in figure 10. (a): 2 mm; (b): 6 mm; (c): 10 mm; (d): 14 mm.

In all of the contour plots of figure 8 there are strong signals around 260 nm and 300–340 nm, independent of input chirp. These are due to third harmonic generation, phase matched between the fundamental and higher order modes [38].

6. Pulse compression and generation of NRR

In the previous section we have found that a compressing incoming pulse undergoes spectral expansion which reaches far into the UV. In particular, it is reaching the wavelength of NRR, thus allowing an excitation of NRR. Figure 9 shows contour plots of UV spectra around the NRR wavelength of 226 nm, as the input pulse chirp is varied, for four fiber lengths.

For all fiber lengths the NRR peak is small for negative and small positive chirps, where the pulse compresses efficiently at the start of fiber propagation. Then it grows to a maximum for a particular chirp, before decreasing. Unsurprisingly, no NRR is generated beyond a chirp leading to pulse compression at the very end of the fiber. The chirp at which the NRR peak reaches its maximum is indicated by a black line in figure 9 and its numerical value is listed in table 1. For the two longer fibers, maximum NRR occurs approximately for compression at the end of the fiber instead of at the much smaller chirp of maximum compression (see figure 6). In the case of the two shorter fibers the maximum NRR is observed for a chirp for compression just before the end of the fiber. This can be explained by figure 10 , which displays the observed NRR signal strength at different fiber lengths for a range of input pulse chirps. Depending on

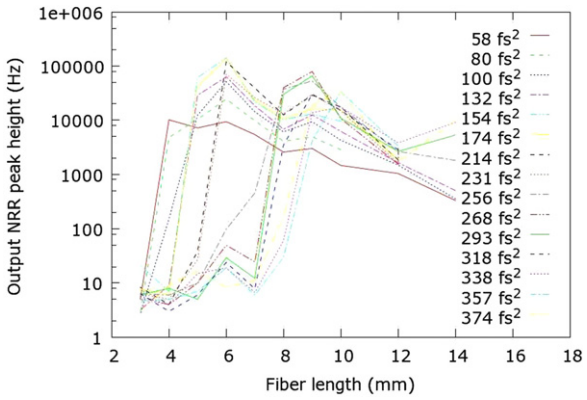

Figure 10. NRR production along the fiber under various input chirps. NRR is most efficiently produced around 6 mm and decays rapidly along the fiber.

the chirp, the pulses compress in the fiber at various distances. It is only during the compression that significant amounts of NRR are generated, after which the UV radiation in the fiber quickly decays. From these data we estimate a UV loss coefficient at 226 nm of 1.5–2.5 dB mm^{-1}. It is also visible in the figure that NRR production further along the fiber is less efficient, with the optimal fiber length close to 6 mm. This again is a result of the less efficient spectral expansion, cf figure 3.

In conclusion we see that it is possible to use the input pulse chirp as a tool to investigate pulse propagation along a fiber. In particular, we observe pulse compression and the evolution of NRR. By delaying the pulse compression to the end of the fiber we observe spectral broadening into the UV, which is required to excite the NRR. Significant NRR is observed only if the pulse compresses near the fiber end because of fiber loss in the UV. In both the simulations and the experiments the degree of pulse compression decreases as the input chirp becomes large and positive. Thus we measure the strongest NRR output for a short fiber, at a chirp that simultaneously optimizes pulse compression and delays the compression towards the fiber end.

The simulations indicate that the deterioration in the pulse compression with increasing chirp is a persistent feature for a variety of input pulse powers and pulse lengths. Therefore choosing an appropriate combination of short fiber and input chirp is crucial in any experiment to generate light in the UV. This is important for a variety of fs-pulsed experiments such as the creation of supercontinua, the generation of RR at short wavelength, or the observation of quantum vacuum radiation from artificial optical event horizons [39, 25, 40].

Other radiation processes based on ultrashort pulse compression can be investigated using the same method, such as the generation of RR.

Acknowledgments

We would like to acknowledge useful discussions with F Biancalana, R Paschotta, and S Kehr.

References

[1] Rubino E, McLenaghan J, Kehr S C, Belgiorno F, Townsend D, Rohr S, Kuklewicz C E, Leonhardt U, König F and Faccio D 2012 Negative-frequency resonant radiation *Phys. Rev. Lett.* **108** 253901–5

[2] Rubino E, Lotti A, Belgiorno F, Cacciatori S L, Couairon A, Leonhardt U and Faccio D 2012 Soliton-induced relativistic-scattering and amplification *Sci. Rep.* **2** 932

[3] Akhmediev N and Karlsson M 1995 Cherenkov radiation emitted by solitons in optical fibers *Phys. Rev.* A **51** 2602–7

[4] Wai P K A, Menyuk C R, Lee Y C and Chen H H 1986 Nonlinear pulse propagation in the neighborhood of the zero-dispersion wavelength of monomode optical fibers *Opt. Lett.* **11** 464–6

[5] Alfano R R and Shapiro S L 1970 Observation of self-phase modulation and small-scale filaments in crystals and glasses *Phys. Rev. Lett.* **24** 592–4

[6] Dudley J M, Genty G and Coen S 2006 Supercontinuum generation in photonic crystal fiber *Rev. Mod. Phys.* **78** 1135–84

[7] Agrawal G P 2001 *Nonlinear Fiber Optics* 3rd edn, ed P L Kelley *et al* (San Diego, CA: Academic Press) p 49

[8] Russell P 2003 Photonic crystal fibers *Science* **299** 358–62

[9] Tu H and Boppart S A 2013 Coherent fiber supercontinuum for biophotonics *Laser Photonics Rev.* **7** 628–45

[10] Chang G *et al* 2012 Spectrally flat broadband visible-wavelength astro-comb *Conference on Lasers and Electro-Optics (San Jose, 6–11 May 2012)*

[11] Tran T X, Cassemiro K N, Söller C, Blow K J and Biancalana F 2011 Hybrid squeezing of solitonic resonant radiation in photonic crystal fibers *Phys. Rev.* A **84** 013824–5

[12] Birrell N D and Davies P C W 1984 *Quantum Fields in Curved Space* (Cambridge: Cambridge University Press)

[13] Hawking S W 1974 Black-hole evaporation *Nature* **248** 30–31

[14] Hawking S W 1975 Particle creation by black holes *Commun. Math. Phys.* **43** 199–220

[15] Unruh W G 1981 Experimental black-hole evaporation? *Phys. Rev. Lett.* **46** 1351–3

[16] Weinfurtner S, Tedford E W, Penrice M C J, Unruh W G and Lawrence G A 2011 Measurement of stimulated Hawking emission in an analogue system *Phys. Rev. Lett.* **106** 021302–5

[17] Barceló C, Liberati S and Visser M 2003 Towards the observation of Hawking radiation in Bose–Einstein condensates *Int. J. Mod Phys. B.* **18** 3735–45

[18] Philbin T G, Kuklewicz C, Robertson S, Hill S, König F and Leonhardt U 2008 Fiber-optical analog of the event horizon *Science* **319** 1367–70

[19] Belgiorno F, Cacciatori S L, Clerici M, Gorini V, Ortenzi G, Rizzi L, Rubino E, Sala V G and Faccio D 2010 Hawking radiation from ultrashort laser pulse filaments *Phys. Rev. Lett.* **105** 203901–4

[20] Nation P D, Johansson J R, Blencowe M P and Nori F 2012 Colloquium: stimulating uncertainty: amplifying the quantum vacuum with superconducting circuits *Rev. Mod. Phys.* **84** 1–24

[21] Choudhary A and König F 2012 Efficient frequency shifting of dispersive waves at solitons *Opt. Express* **20** 5538–46

[22] Chang G, Chen L and Kärtner F X 2010 Highly efficient Cherenkov radiation in photonic crystal fibers for broadband visible wavelength generation *Opt. Lett.* **35** 2361–3

[23] Roy S, Bhadra S K and Agrawal G P 2009 Dispersive waves emitted by solitons perturbed by third-order dispersion inside optical fibers *Phys. Rev.* A **79** 023824–9

[24] Tu H and Boppart S A 2009 Optical frequency up-conversion by supercontinuum-free widely-tunable fiber-optic Cherenkov radiation *Opt. Express* **17** 9858–72

[25] Tu H and Boppart S A 2009 Ultraviolet-visible non-supercontinuum ultrafast source enabled by switching single silicon strand-like photonic crystal fibers *Opt. Express* **17** 17983–8

[26] Cheng C, Wang Y and Qinghua L 2011 Effect of initial frequency chirp on the supercontinuum generation in all-normal dispersion photonic crystal fibers *Proc. of the SPIE, Photonics and Optoelectronics Meetings*

(POEM) Optical Communication Systems and Networking ed Z Zhao, R Penty, C Shu and T Jiang (Wuhan, China) vol 8331 83310O

[27] Fu X, Qian L, Wen S and Fan D 2004 Nonlinear chirped pulse propagation and supercontinuum generation in microstructured optical fiber *J. Opt. A: Pure Appl. Opt.* **6** 1012–6

[28] Zhang H, Yu S, Zhang J and Gu W 2007 Effect of frequency chirp on supercontinuum generation in photonic crystal fibers with two zero-dispersion wavelengths *Opt. Express* **15** 1147–54

[29] Zhu Z and Brown T 2004 Effect of frequency chirping on supercontinuum generation in photonic crystal fibers *Opt. Express* **12** 689–94

[30] Tianprateep M, Tada J and Kannari F 2005 Influence of polarization and pulse shape of femtosecond initial laser pulses on spectral broadening in microstructure fibers *Opt. Rev.* **12** 179–89

[31] Tianprateep M, Tada Ji, Yamazaki T and Kannari F 2004 Spectral-shape-controllable supercontinuum generation in microstructured fibers using adaptive pulse shaping technique *Japan J. Appl. Phys.* **43** 8059–63

[32] Herrmann J, Griebner U, Zhavoronkov N, Husakou A, Nickel D, Knight J C, Wadsworth W J, Russell P St J and Korn G 2002 Experimental evidence for supercontinuum generation by fission of higher-order solitons in photonic fibers *Phys. Rev. Lett.* **88** 173901–4

[33] Husakou A V and Herrmann J 2001 Supercontinuum generation of higher-order solitons by fission in photonic crystal fibers *Phys. Rev. Lett.* **87** 203901–4

[34] Cristiani I, Tediosi R, Tartara L and Degiorgio V 2004 Dispersive wave generation by solitons in microstructured optical fibers *Opt. Express* **12** 124–35

[35] Skryabin D V and Yulin A V 2005 Theory of generation of new frequencies by mixing of solitons and dispersive waves in optical fibers *Phys. Rev.* E **72** 016619

[36] Conforti M, Marini A, Tran T, Faccio D and Biancalana F 2013 Interaction between optical fields and their conjugates in nonlinear media *Opt. Express* **21** 31239–52

[37] Paschotta R 2008 *Simulation Software PROPULSE* (Zurich: RP Photonics Consulting GmbH)

[38] Efimov A, Taylor A, Omenetto F, Knight J, Wadsworth W and Russell P 2003 Phase-matched third harmonic generation in microstructured fibers *Opt. Express* **11** 2567–76

[39] Price J H V, Monro T M, Furusawa K, Belardi W, Baggett J C, Coyle S, Netti C, Baumberg J J, Paschotta R and Richardson D J 2003 UV generation in a pure-silica holey fiber *Appl. Phys.* B **77** 291–8

[40] Leonhardt U and Robertson S 2012 Analytical theory of Hawking radiation in dispersive media *New J. Phys.* **14** 053003